International Journal of Fluid Mechanics Research, Vol. 27, Nos. 2–4, 2000

Hydromagnetic Flow and Heat Transfer of a Particulate Suspension Over a Non-Isothermal Surface with Variable Properties

A. J. Chamkha
Department of Mechanical and Industrial Engineering
Kuwait University
Safat, Kuwait

A numerical study of steady, laminar, hydromagnetic, boundary-layer flow and heat transfer of a particulate suspension exhibiting finite particle volume fraction over a non-isothermal semi-infinite flat plate with variable properties is performed using a modified dusty-gas model. This modified model allows for particle-phase stresses, magnetic field and heat generation or absorption effects. The development of the displacement thicknesses and the skin-friction coefficients of both phases, as well as the wall particle-phase tangential velocity and the wall heat transfer coefficient are illustrated graphically for various parametric conditions. The results indicate that the presence of a transverse magnetic field causes the displacement thicknesses of both phases to decrease over the whole of the computational domain while the skin-friction coefficients of both phases and the wall heat transfer coefficient increase.

* * *

Introduction

This work is concerned with the study of the flow and heat transfer aspects of steady, laminar, boundary-layer and variable properties flow of a particulate suspension in an electrically-conducting and heat-generating or absorbing fluid past a non-isothermal semi-infinite flat plate in the presence of a transverse magnetic field moving at the free stream velocity. This is a fundamental problem in fluid-particle mechanics which has received little attention. In addition, the problem under consideration may find many applications such as fluidized beds, gas purification, conveying of powdered materials and transport processes, environmental pollutant motions, cooling of nuclear reactors and geothermal systems where the working fluid is electrically conducting and its properties vary with temperature. This is especially true for high temperature operations. Other than the contributions of the present author, the only major previous works on special cases of this problem have been reported some time ago by Singleton (1965) and Wang and Glass (1988). Both of these references considered compressible flow of electrically nonconducting fluids with suspended solid particles over an isothermal plate in the absence of magnetic field, heat generation, and parti-

ISSN 1064-2277

cle-phase viscous effects. Singleton (1965) obtained asymptotic solutions using the series expansion method for both the small slip region (where the particle slip velocity is small) far down stream of the leading edge of the plate and the large-slip region (where the slip velocity between the two phases is large) close to the leading edge of the plate. Singleton (1965) assumed that both the density of the fluid phase and that of the particle phase were not constant. Furthermore, he assumed that the fluid viscosity is proportional to the square root of its temperature. Wang and Glass (1988), on the other hand, considered a moderate-slip region (or a non-equilibrium transition region) in addition to the large- and small-slip regions. They obtained asymptotic series expansion results in all these regions as well as a finite difference solution over the whole plate. In their investigation, Wang and Glass (1988) employed a more general viscosity-temperature power-law relation and considered cases for Stokes and non-Stokes drag forces. Similar to Singleton (1965), Wang and Glass (1988) allowed both densities of the fluid and particle phases to vary and assumed small particulate volume fraction following Marble (1970) and Soo (1989). Chamkha (1996a, b) has also considered compressible dusty-gas flow over an isothermal flat plate with small and finite particulate volume fractions for electrically non-conducting and thermally neutral fluids in the absence of a magnetic field. Also, there is some literature on the incompressible version of this problem reported by many authors such as Soo (1968), Osiptsov (1980), Prabha and Jain (1980), Datta and Mishra (1982), and Chamkha and Peddieson (1989, 1992). In the present work, a dusty-gas model with an externally imposed magnetic field, heat generation or absorption, finite volume fraction of particles, endowing the particle phase by an artificial viscosity (see, for instance, Gidaspow, 1986, Gadiraju et al., 1992, and Chamkha and Peddieson, 1994) is developed for the solution of compressible flow and heat transfer over a non-isothermal horizontal surface.

Mathematical Formulation

Consider a steady, two-dimensional, hydromagnetic, compressible flow in the x, y-plane over a semi-infinite plate $y = 0$, $x > 0$ and heat transfer of a two-phase particulate suspension with heat generation or absorption. A transverse magnetic field which varies with the distance along the plate such that $B(x) = B_0 x^{-1/2}$ (where B_0 is a constant) and moves with the free stream is applied in the direction normal to the plate. Far from the plate, the flow is a uniform stream in the x-direction parallel to the plate. Because of the difference in the wall velocity and temperature values and those of the free stream, and due to viscous and thermal diffusion effects, hydrodynamic and thermal boundary layers develop along the plate. As opposed to a previous investigation (Singleton, 1965) of this problem, the suspension is somewhat dense and the particles are assumed to be spheres of one finite size. This necessitates the consideration of a dusty-gas model including particle-phase viscous stresses (which may represent particle-particle interaction) and finite particle volume fraction. A boundary-layer dimensional analysis similar to that discussed by Chamkha and Peddieson (1990, 1994) shows that the particle-phase density in the boundary layer is uniform. In this analysis, the boundary layer equations simplify to

$$\frac{\partial}{\partial x}(\rho u) + \frac{\partial}{\partial y}(\rho v) = 0 \tag{1}$$

$$\rho\left(u\frac{\partial u}{\partial x} + v\frac{\partial u}{\partial y}\right) = \frac{\partial}{\partial y}\left(\mu\frac{\partial u}{\partial y}\right) + \rho_p N(u_p - u) - \sigma B(x)^2(u - u_\infty) \tag{2}$$

$$c\rho\left(u\frac{\partial T}{\partial x}+\nu\frac{\partial T}{\partial y}\right) = \frac{\partial}{\partial y}\left(k\frac{\partial T}{\partial y}\right)+\mu\left(\frac{\partial u}{\partial y}\right)^2+\rho_p N(u_p-u)^2$$
$$+ c_p\rho_p N_T(T_p-T)+Q^*(x)(T-T_\infty) \tag{3}$$

$$P = \rho RT \tag{4}$$

$$\rho_p\left(u_p\frac{\partial u_p}{\partial x}+\nu_p\frac{\partial u_p}{\partial y}\right) = \frac{\partial}{\partial y}\left(\mu_p\frac{\partial u_p}{\partial y}\right)-\rho_p N(u_p-u) \tag{5}$$

$$\rho_p\left(u_p\frac{\partial \nu_p}{\partial x}+\nu_p\frac{\partial \nu_p}{\partial y}\right) = \frac{\partial}{\partial y}\left(\mu_p\frac{\partial \nu_p}{\partial y}\right)-\rho_p N(\nu_p-\nu) \tag{6}$$

$$c_p\rho_p\left(u_p\frac{\partial T_p}{\partial x}+\nu_p\frac{\partial T_p}{\partial y}\right) = \mu_p\left(\frac{\partial u_p}{\partial y}\right)^2-c_p\rho_p N_T(T_p-T) \tag{7}$$

where ρ, u, ν, P and T represent the fluid-phase density, velocity component in the x-direction, velocity component in the y-direction, pressure, and temperature, respectively. μ, c, k and R are the fluid-phase dynamic viscosity, electrical conductivity, specific heat, thermal conductivity, and gas constant, respectively. T_∞ is the free stream temperature, $B(x)$ is the magnetic induction, $Q^*(x)$ is the heat generation (> 0) or absorption (< 0) coefficient, and the subscript p refers to the same variable for the particle phase. $N = 18\mu/(\rho_s d^2)$ and $N_T = 12k/(\rho_s d^2 c_p)$ (where ρ_s and d are the density for the particle material and the particle diameter, respectively) are the momentum and heat transfer coefficients, respectively. The fluid phase is assumed to be electrically conducting, while the particle phase and the stationary plate are assumed to be electrically insulating. In addition, no electric field is assumed to exist and the magnetic Reynolds number is assumed to be small so that the induced magnetic field is neglected. In the present study Q^* is assumed to vary with the distance along the plate according to $Q^*(x) = Q_0/x$ where Q_0 is a constant.

Equations (1) through (7) represent the fluid-phase balances of mass, linear momentum in the x-direction, energy, and equation of state (since the fluid is assumed to behave as a perfect gas), and the particle-phase balances of linear momentum in the x- and y-directions, and energy, respectively. These two-phase equations are coupled together through drag and heat transfer. The drag force is modeled by Stokes linear drag theory and the particle phase similar to the fluid phase is treated as a continuum having a viscosity.

The viscous dissipation terms in the energy equations of both phases are not neglected in this work. To obtain closure of the governing equations, a knowledge about the dependence of the viscosities of both phases as well as the thermal conductivity of the fluid phase on flow variables is needed. Following Wang and Glass (1988), both the viscosity of the fluid phase and that of the particle phase may be represented, respectively, as

$$\frac{\mu}{\mu_\infty} = \left(\frac{T}{T_\infty}\right)^\omega \qquad \frac{\sigma}{\sigma_\infty} = \left(\frac{T}{T_\infty}\right)^\omega \quad (0.5 \le \omega \le 1.0) \tag{8a, b}$$

$$\frac{\mu_p}{\mu_{p\infty}} = \left(\frac{T_p}{T_\infty}\right)^{\omega_p} \quad (0.5 \le \omega_p \le 1.0) \tag{8c}$$

where and ω_p are power index coefficients for the fluid and the particle phases, respectively, σ_∞ is the free-stream electrical conductivity of the fluid, and μ_∞ and $\mu_{p\infty}$ are the free-stream fluid- and particle-phase viscosity coefficients, respectively. Both phases are assumed to have the same power index coefficient. This was done because when ω and ω_p were not equal, small variations in the results were predicted from those corresponding to the case when ω and ω_p were equal.

The physics of this problem suggest the following boundary conditions:

$$u(x,0) = 0 \qquad v(x,0) = 0 \qquad T(x,0) = T_0(x)$$

$$\frac{\partial u_p}{\partial y}(x,0) = Su_p(x,0) \qquad v_p(x,0) = 0$$

$$u(x,\infty) = U_\infty \qquad u_p(x,\infty) = U_\infty \qquad v_p(x,\infty) = v(x,\infty)$$

$$T(x,\infty) = T_\infty \qquad T_p(x,\infty) = T_\infty \qquad \rho(x,\infty) = \rho_\infty \tag{9}$$

where ρ_∞, U_∞, T_0, and S are the free-stream density and velocity, fluid-phase variable wall temperature, and particle-phase wall slip, respectively. The fourth equation in Eqs. (9) is borrowed from rarefied gas dynamics since the particle phase may behave as a rarefied gas.

The dimensionless equations may be obtained from modified Blasius transformations (Chamkha, 1996a)

$$x = \frac{U_\infty \xi}{N(1-\xi)} \qquad y = \frac{U_\infty}{N\mathrm{Re}_\infty^{1/2}}\left(\frac{2\xi}{1-\xi}\right)^{1/2}\eta$$

$$u = U_\infty F \qquad v = U_\infty\left(\frac{1-\xi}{2\xi}\right)^{1/2}(G+\eta F)/\mathrm{Re}_\infty^{1/2}$$

$$u_p = U_\infty F_p \qquad v_p = U_\infty\left(\frac{1-\xi}{2\xi}\right)^{1/2}(G_p+\eta F_p)/\mathrm{Re}_\infty^{1/2}$$

$$T = T_\infty\theta \qquad T_p = T_\infty\theta_p \qquad \rho = \rho_\infty Q \qquad \rho_p = \rho_{p\infty} = \rho_\infty$$

$$\mu = \mu_\infty\Gamma \qquad \mu_p = \mu_{p\infty}\Gamma_p$$

$$\mathrm{Pr} = \frac{\mu c}{k} \qquad \mathrm{Ec} = \frac{U_\infty^2}{cT_\infty} \qquad \beta = \frac{\mu_{p\infty}}{\mu_\infty} \qquad \gamma = \frac{c}{c_p}$$

$$\mathrm{Ha}^2 = \frac{\sigma_\infty B_0^2}{\rho_\infty N} \qquad \alpha = \frac{Q_0}{\rho_\infty cN} \tag{10}$$

(where $\mathrm{Re}_\infty = \rho_\infty U^2{}_\infty/(N\mu_\infty)$) along with Eqs. (8) into Eqs. (1) through (7) to yield

$$\frac{\partial(QG)}{\partial\eta} + QF + 2\xi(1-\xi)\frac{\partial(QF)}{\partial\xi} = 0 \tag{11}$$

$$\Gamma\frac{\partial^2 F}{\partial\eta^2} + \left(\frac{d\Gamma\partial\theta}{d\theta\partial\eta} - QG\right)\frac{\partial F}{\partial\eta} - 2\mathrm{Ha}^2\Gamma(F-1)$$

$$-\frac{2\xi}{1-\xi}\left((1-\xi)^2 QF\frac{\partial F}{\partial \xi}-\Gamma(F_p-F)\right)=0 \tag{12}$$

$$\Gamma\frac{\partial^2\theta}{\partial\eta^2}+\left(\frac{d\Gamma\partial\theta}{d\theta\partial\eta}-\mathrm{Pr}QG\right)\frac{\partial\theta}{\partial\eta}-2\xi(1-\xi)\mathrm{Pr}QF\frac{\partial\theta}{\partial\xi}+\mathrm{PrEc}\Gamma\left(\frac{\partial F}{\partial\eta}\right)^2$$
$$+2\alpha\mathrm{Pr}(\theta-1)+\left(\frac{2\xi}{1-\xi}\right)\left(\mathrm{PrEc}\Gamma(F_p-F)^2+\frac{2\Gamma}{3}(\theta_p-\theta)\right)=0 \tag{13}$$

$$Q=\frac{1}{H} \tag{14}$$

$$\beta\Gamma_p\frac{\partial^2 F_p}{\partial\eta^2}+\left(\beta\frac{d\Gamma_p}{d\theta_p}\frac{\partial\theta_p}{\partial\eta}-G_p\right)\frac{\partial F_p}{\partial\eta}-\left(\frac{2\xi}{1-\xi}\right)\Gamma(F_p-F)$$
$$-2\xi(1-\xi)F_p\frac{\partial F_p}{\partial\xi}=0 \tag{15}$$

$$\beta\Gamma_p\frac{\partial^2}{\partial\eta^2}(G_p+\eta F_p)+\beta\frac{d\Gamma_p}{d\theta_p}\frac{\partial\theta_p}{\partial\eta}\frac{\partial}{\partial\eta}(G_p+\eta F_p)$$
$$-G_p\frac{\partial G_p}{\partial\eta}-\eta G_p\frac{\partial F_p}{\partial\eta}+\eta F_p^2-2\xi(1-\xi)F_p\frac{\partial}{\partial\xi}(G_p+\eta F_p)$$
$$-\left(\frac{2\xi}{1-\xi}\right)\Gamma(G_p-G+\eta(F_p-F))=0 \tag{16}$$

$$G_p\frac{\partial\theta_p}{\partial\eta}-\beta\mathrm{Ec}\gamma\Gamma_p\left(\frac{\partial F_p}{\partial\eta}\right)^2+2\xi(1-\xi)F_p\frac{\partial\theta_p}{\partial\xi}+\left(\frac{4\xi}{1-\xi}\right)\frac{\gamma\Gamma}{3\mathrm{Pr}}(\theta_p-\theta)=0 \tag{17}$$

The boundary conditions become

$$F(\xi,0)=0 \qquad G(\xi,0)=0 \qquad \theta(\xi,0)=t_0\xi^n$$
$$\frac{\partial F_p}{\partial\eta}(\xi,0)=S\left(\frac{2\xi}{1-\xi}\right)^{1/2}F_p(\xi,0) \qquad G_p(\xi,0)=0$$
$$F(\xi,\infty)=1 \qquad F_p(\xi,\infty)=1 \qquad G_p(\xi,\infty)=G(\xi,\infty)$$
$$\theta(\xi,\infty)=1 \qquad \theta_p(\xi,\infty)=1 \qquad Q(\xi,\infty)=1 \tag{18}$$

where t_0 is a dimensionless fluid-phase wall temperature and the constant n is the wall temperature power index coefficient.

The particle-phase wall tangential velocity is controlled by a variety of physical effects. These include sliding friction, the nature of particle-surface interaction and others. It is not possible to measure or model such effects with precision at present. In the present work, however, various particle-phase wall velocity conditions are allowed. Thus, it was assumed that the wall slip parameter for the particle phase S to be a function of the wall position ξ, since the wall slip velocity is dependent on ξ. A general function of the form

$$S = S_r\left(\frac{\xi}{1-\xi}\right)^r \tag{19}$$

(where S_r and r (> 0) are constants) is employed in the present work. It can be seen that the form of Eq. (19) allows perfect wall slip at $\xi = 0$ followed by a transition or approach to no-slip far down-stream of the plate's leading edge at a rate controlled by the values of S_r and r.

The fluid-phase displacement thickness Δ, the particle-phase displacement thickness Δ_p, fluid-phase skin-friction coefficient C, the particle-phase displacement thickness C_p, and the wall heat transfer coefficient q_w are defined, respectively, as

$$\Delta(\xi) = \int_0^\infty (1 - QF)d\eta \qquad \Delta_p(\xi) = \int_0^\infty (1 - F_p)d\eta \qquad C(\xi) = \Gamma(\xi, 0)\frac{\partial F}{\partial \eta}(\xi, 0)$$

$$C_p(\xi) = \beta\Gamma_p(\xi, 0)\frac{\partial F_p}{\partial \eta}(\xi, 0) \qquad q_w(\xi) = \frac{\Gamma(\xi, 0)}{\mathrm{EcPr}}\frac{\partial \theta}{\partial \eta}(\xi, 0) \tag{20}$$

Results and Discussion

The numerical results were computed using an iterative, implicit, tri-diagonal finite-difference scheme (see, for instance, Blottner, 1970, and Patankar, 1980). Attention will be focused on the influence of the particle-phase wall slip coefficient S, Hartmann number Ha, and the heat generation/absorption coefficient.

All first order-derivatives with respect to are represented by two-point backward difference formulas. All second-order differential equations in are discretized using three-point central differences while all first-order differential equations in are discretized using the trapezoidal rule. The computational domain was divided into 1001 nodes in the direction and 195 nodes in the direction. Since it expected that most changes in the boundary layer occur in the vicinity of the wall, increasing mesh intervals are used starting from $\Delta\eta_1 = 0.001$ with a growth factor of 1.03. Also, constant small step sizes in ξ with $\Delta\xi = 0.001$ are used. The governing equations are then converted into sets of linear tri-diagonal algebraic equations which are solved by the Thomas Algorithm (see, Blottner, 1970) at each iteration. The convergence criterion is 10^{-5} in the difference between the current and the previous iterations. It should be mentioned that many numerical simulations were performed by altering the step sizes in both directions to ensure that the results are accurate and independent of the grid size. For example, when $\Delta\eta_1$ was set to 0.01 instead 0.001, an average error of about 8% was observed in the results with the maximum error being close to $\xi = 1$. Also, when $\Delta\eta_1$ was 0.0001 no significant changes of results were observed. For this reason $\Delta\eta_1 = 0.001$ was retained. The flow and heat transfer parameter are not as sensitive to $\Delta\xi$ as they are sensitive to $\Delta\eta_1$. For this reason, a constant step size was used in the ξ direction. The sensitivity analysis of the results to changes in $\Delta\xi$ was also performed. For instance, when $\Delta\xi$ was set to 0.01, an average deviation of 5% from the results with $\Delta\xi$ = 0.001. Smaller values of $\Delta\xi$ than 0.01 produced no changes in the results and, therefore, $\Delta\xi$ was set to 0.001 in all the produced results. As far as the convergence criterion is concerned, two types were tried. One was based on the percentage error between the previous and the current iterations and the other was based on their difference. Since we are not dealing with very small numbers, the convergence criterion based on the difference between the previous and current iterations was employed in the present study. No convergence problems were encountered even with the small value of 10^{-5} used

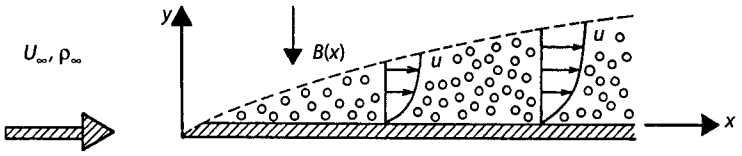

Fig. 1. Geometry and coordinate system.

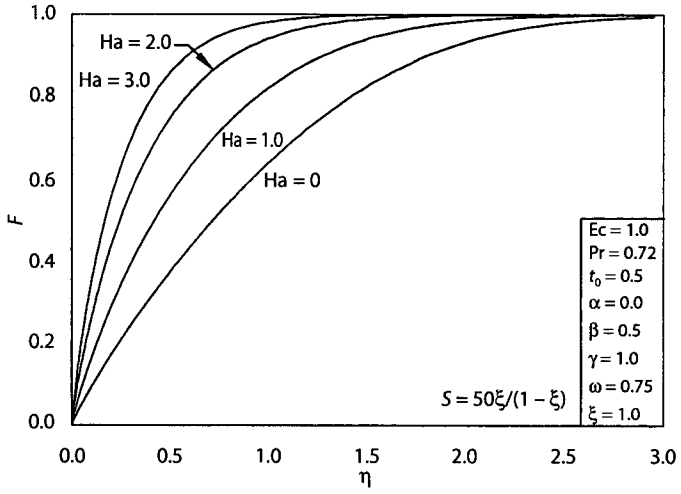

Fig. 2. Effects of Ha on fluid-phase tangential velocity.

in this work. A representative set is presented in Figs. 2 through 18 to show the effects of the Hartmann number Ha, particle-phase wall slip coefficient S and the heat generation or absorption coefficient α, on the flow and heat transfer properties of the problem.

Figure 2 through 5 present representative profiles for the fluid-phase tangential velocity F, particle-phase tangential velocity F_p, fluid-phase temperature θ and particle-phase temperature θ_p for various values of the Hartmann number Ha at the tangential distance $\xi = 1$, respectively. These results correspond to a viscous particle phase with a wall slip coefficient S exhibited by Eq. (19) with $S_r = 50$ and $r = 1$. Imposition of a transverse magnetic field normal to the flow direction and moving at the free stream velocity creates a tangential motive force. This force acts in the same direction of the flow. Thus, it tends to speed up the movement of the fluid phase and consequently, the particle phase (through the interphase drag force) along the surface. This is accompanied by a reduction in both the fluid- and particle-phase boundary layers. These behaviors are clearly depicted by the increases in the tangential velocities of both phases as Ha increases shown in Figs. 2 and 3. In addition, another result of the imposed magnetic field is the enhancement of both the fluid- and particle-phase temperatures as suggested by the increases in θ and θ_p as Ha increases shown in Figs. 4 and 5. An important observation from Figs. 2 through 5 is that the profiles of F and F_p and the profiles of θ and θ_p are the same at $\xi = 1$ for all values of Ha. This means that both phases are in complete hydrodynamic and thermal equilibrium there.

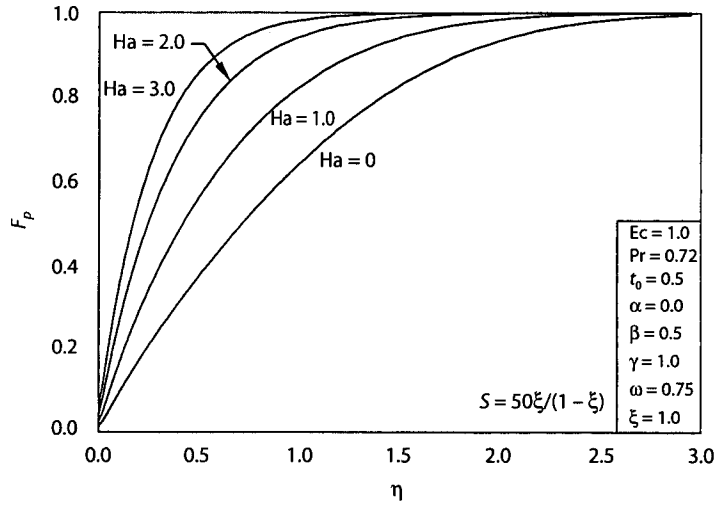

Fig. 3. Effects of Ha on particle-phase tangential velocity.

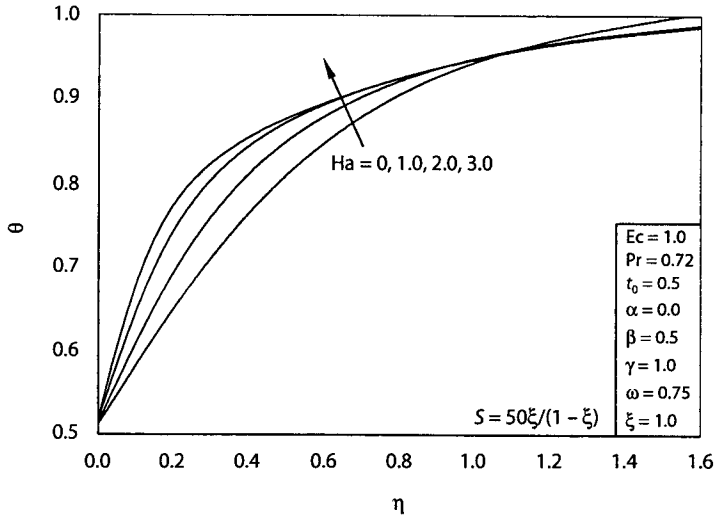

Fig. 4. Effects of Ha on fluid-phase temperature.

Figures 6 through 10 illustrate, respectively, the influence of the Hartmann number Ha on the fluid-phase displacement thickness Δ, the particle-phase displacement thickness Δ_p, the fluid-phase skin-friction coefficient C, the particle-phase skin-friction coefficient C_p and the wall heat transfer coefficient q_w along the plate tangential distance ξ, for the same particle-phase wall slip coefficient S employed in Figs. 2 through 5. It is seen from Figs. 2 and 3 that the presence of the transverse moving magnetic field causes the tangential velocities of both phases to increase. This is true at any fixed tangential position along the plate ξ. This has the tendency to decrease both the fluid- and particle-phase displacement thicknesses Δ and Δ_p at any tangential location along the plate. This

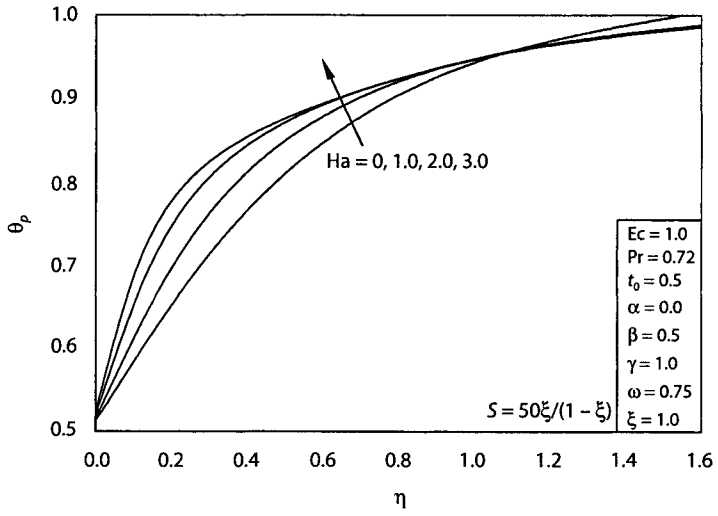

Fig. 5. Effects of Ha on particle-phase temperature.

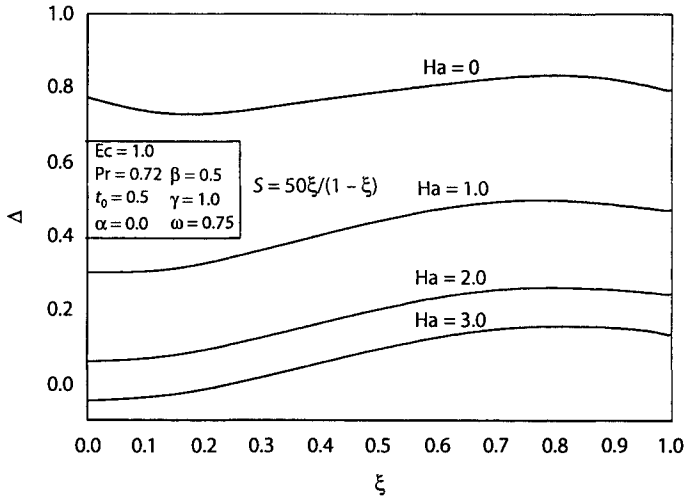

Fig. 6. Effects of Ha on Fluid-phase displacement thickness.

behavior is obvious from Figs. 6 and 7. It should be mentioned that the profile of the tangential velocity of the particle phase F_p is uniform at $\xi = 0$. This means that the value of Δ_p there is zero. However, the fluid-phase tangential velocity profile at $\xi = 0$ is not uniform and is different for different values of Ha. This explains the different values of Δ with at $\xi = 0$ for the different values of Ha employed. It is interesting to observe from Fig. 6 the existence of a small dip in the development of Δ with ξ for Ha = 0 and the increase of Δ with ξ for all other values. From Fig. 7, it is observed that, starting from the leading edge of the plate ($\xi = 0$), Δ_p increases with ξ reaching a maximum and then decreases as ξ approaches unity.

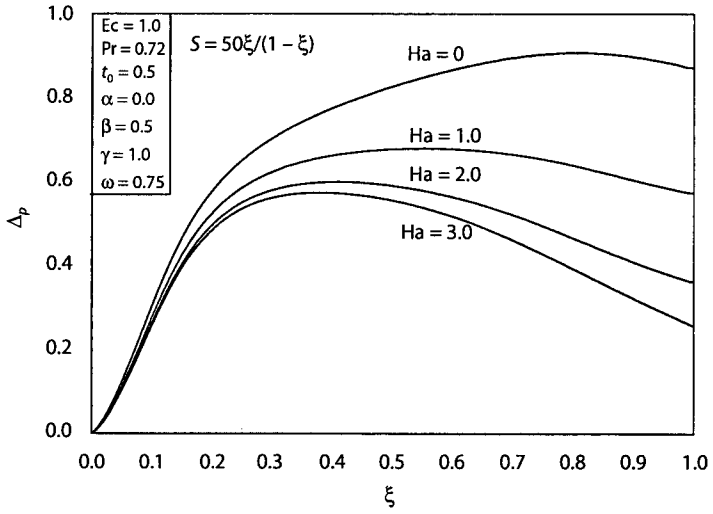

Fig. 7. Effects of Ha on particle-phase displacement thickness.

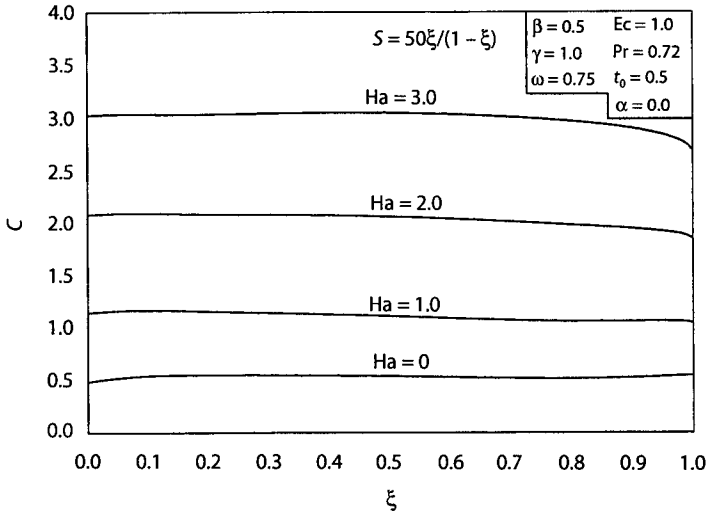

Fig. 8. Effects of Ha on fluid-phase skin-friction coefficient.

Furthermore, Figs. 2 and 3 indicate that the wall slopes of the profiles F and F_p increase as Ha increases resulting in immediate increases in the skin-friction coefficients of both phases C and C_p. This is true for all values of ξ. The value of C_p at $\xi = 0$ is zero while the value of C changes as Ha changes for the same reasons explained before for Δ and Δ_p. It is also predicted that while C changes slightly with ξ, significant variations in the values of C_p with ξ are observed. Inspection of Fig. 4 indicates that the slope of the fluid-phase temperature profile θ increases as Ha increases. As suggested by Eq. (20), this yields an enhancement in the wall heat transfer as shown in Fig. 10. This figure also shows that q_w has an increasing trend with the tangential distance ξ.

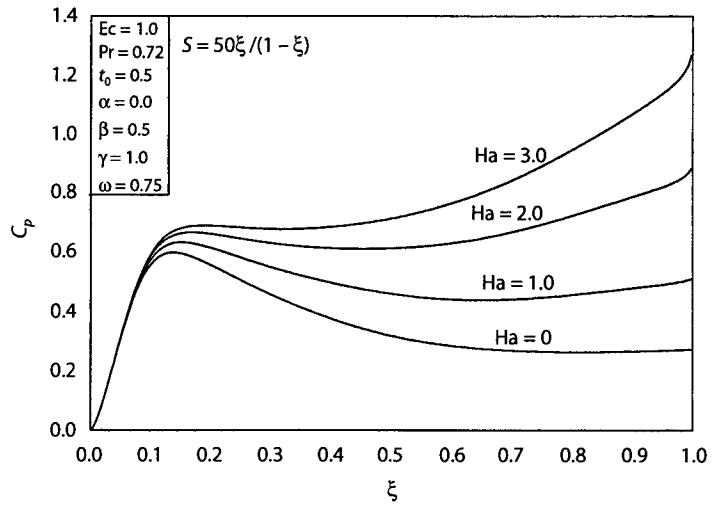

Fig. 9. Effects of Ha on particle-phase skin-friction coefficient.

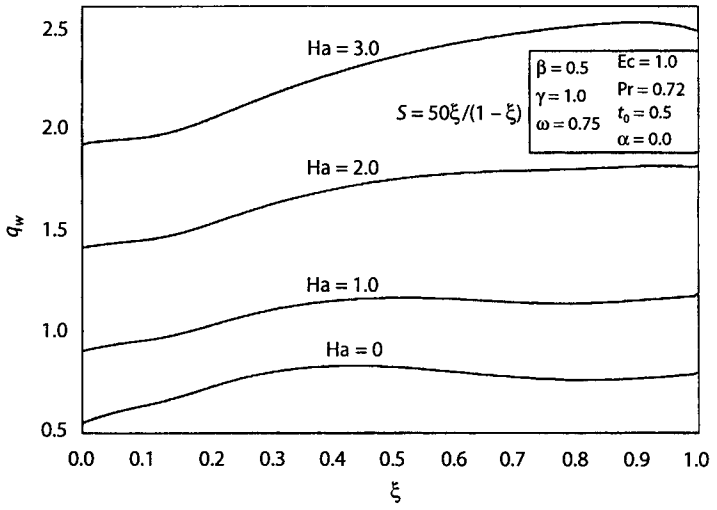

Fig. 10. Effects of Ha on wall heat transfer.

A complete set of numerical results similar to that reported in Figs. 6 through 10 with the addition of Fig. 11 for the development of the wall particle-phase tangential velocity $F_p(\xi, 0)$ with ξ is presented in Fig. 12 through 16 for the uniform particle-phase wall slip coefficient $S = 1.0$, respectively. It is observed from Fig. 11 that $F_p(\xi, 0)$ increases as Ha increases and that the particle phase experiences slip over the whole plate even $\xi = 1.0$. This means that both phases will never be in equilibrium at the wall since the fluid phase experiences a no-slip condition over the surface.

Figures 12 through 16 show similar qualitative features as those reported in Figs. 6 through 10, namely that both Δ and Δ_p decrease while C, C_p and q_w increase due to increases in the strength of

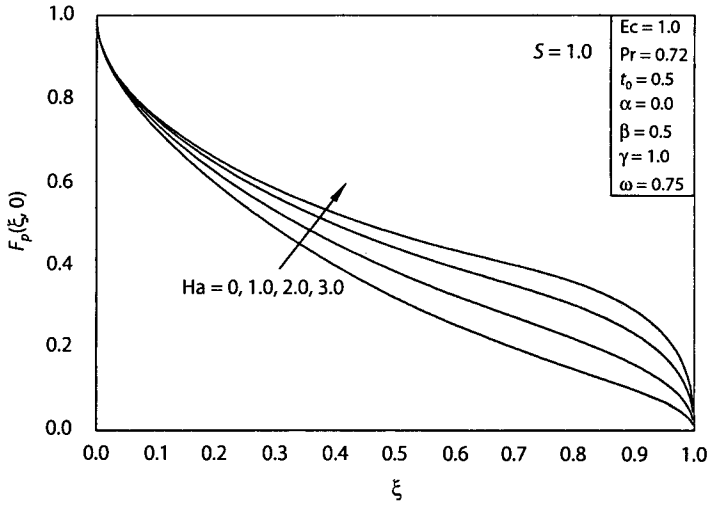

Fig. 11. Effects of Ha on wall particle-phase tangential velocity.

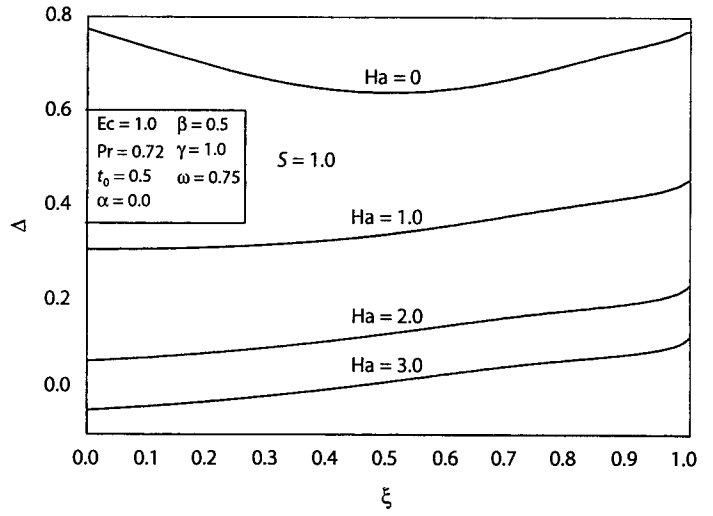

Fig. 12. Effects of Ha on fluid-phase displacement thickness.

the magnetic field. The difference is that all of Δ, C, and q_w are lower while both Δ_p and C_p are higher for $S = 1.0$ than for $S = 50\xi/(1 - \xi)$. Also, the distinctive minimum in the values of Δ for Ha = 0 and the steady increase of Δ_p with ξ, for $S = 1.0$ are worth noting. The purpose of presenting this set of figures in comparison with Figs. 6 through 10 is to show the effects of the particulate wall slip on the results.

Finally, Figs. 17 and 18 illustrate the effects of the heat generation or absorption coefficient α. on the fluid-phase skin-friction coefficient C and the wall heat transfer coefficient q_w for $S = 50\xi/(1 - \xi)$, respectively. Positive values of α indicate heat generation (source) and negative values

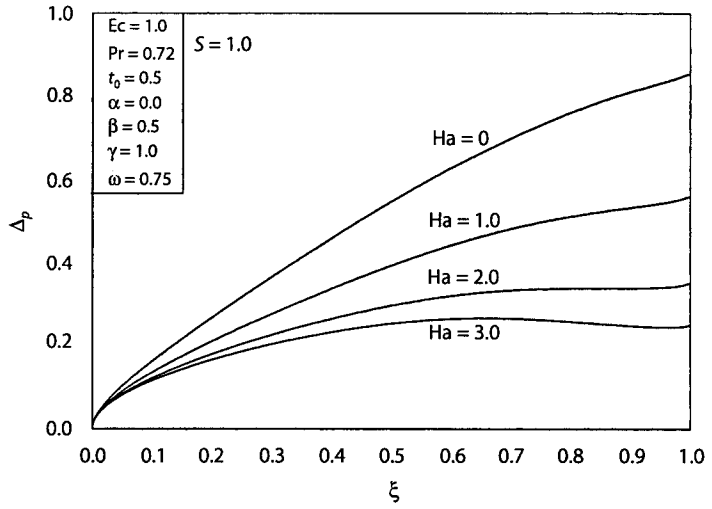

Fig. 13. Effects of Ha on particle-phase displacement thickness.

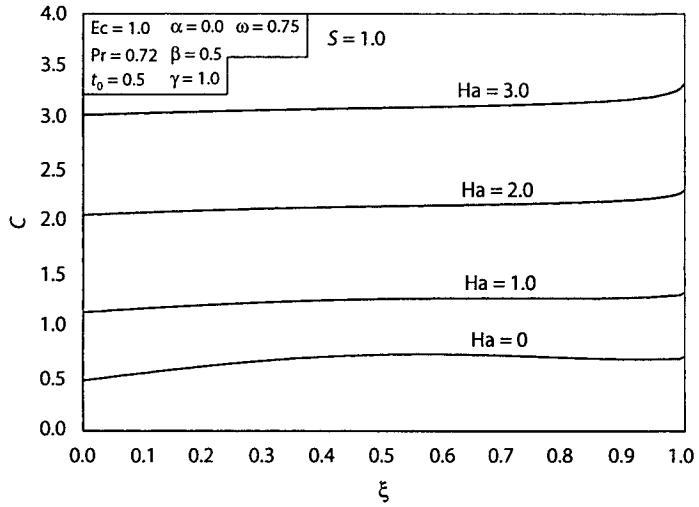

Fig. 14. Effects of Ha on fluid-phase skin-friction coefficient.

of α correspond to heat absorption (sink). It is clearly shown in these figures that while heat generation (α > 0) reduces both the fluid-phase wall friction and wall heat transfer, heat absorption produces the opposite result, namely increases in both C and q_w for essentially all values of ξ. Also, it is observed that both C and q_w respond more to heat generation than to heat absorption. This can be seen from the variations in C and q_w for α = −0.5 and α = 0.5 in comparison with α = 0.

It should be mentioned that no direct comparisons with previously published results on this problem were possible since in all that work the particle-phase density was not constant in the boundary layer and the predictions of the present model are in major contrast with earlier work as far as the density is concerned. Also, no comparisons with experimental data was performed due to

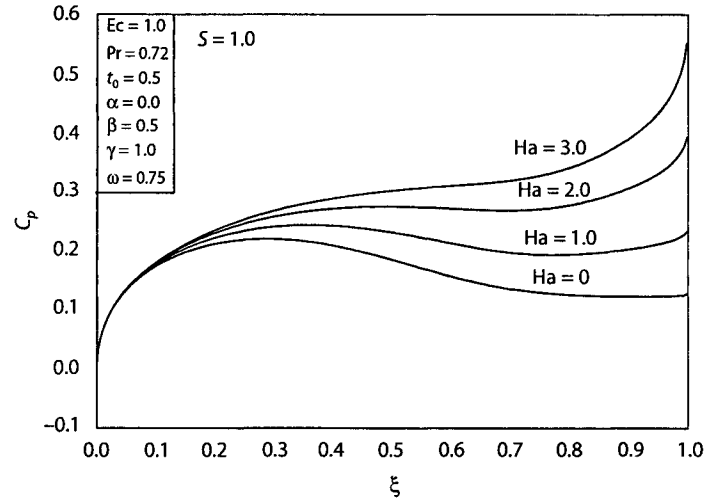

Fig. 15. Effects of Ha on particle-phase skin-friction coefficient.

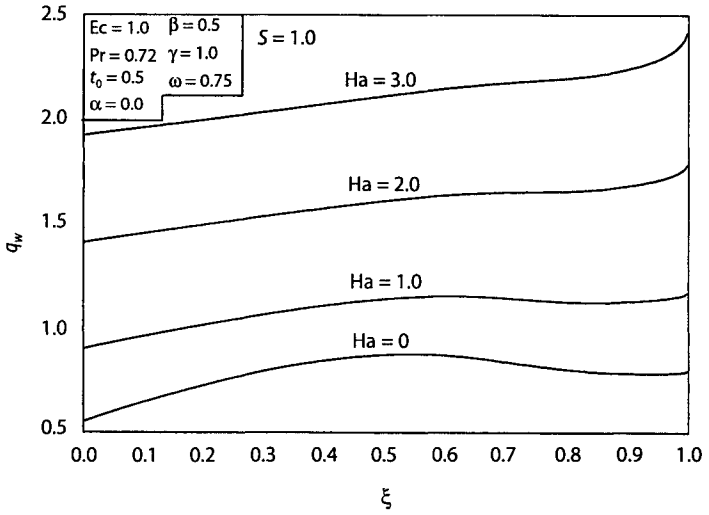

Fig. 16. Effects of Ha on wall heat transfer.

the absence of such data at present. However, with some modifications in the computer program used to obtain the present results, the incompressible results discussed by Chamkha and Peddieson (1994, 1990) for electrically non-conducting and non-generating and non-absorbing fluids were recovered. This helped in verifying the correctness of the numerical results presented in this paper.

In the absence of experimental data on this problem, it is difficult to assess the physical validity of the results presented in this work. It is, therefore, hoped that the theoretical predictions reported herein serve as a stimulus for experimental work on this problem in the future.

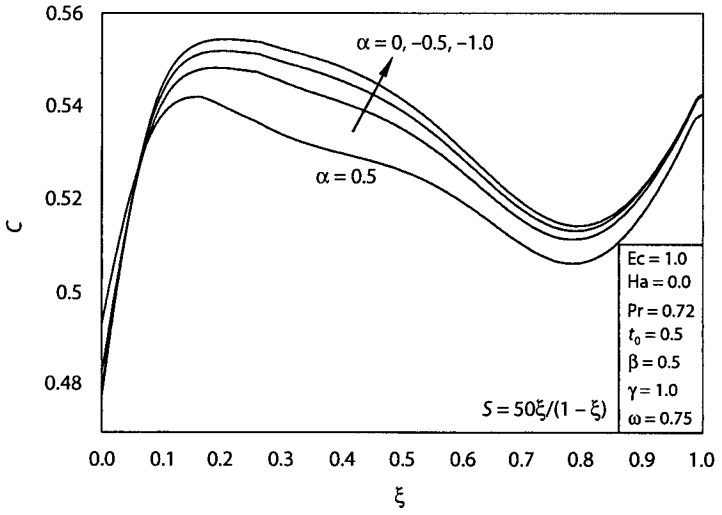

Fig. 17. Effects of α on fluid-phase skin-friction coefficient.

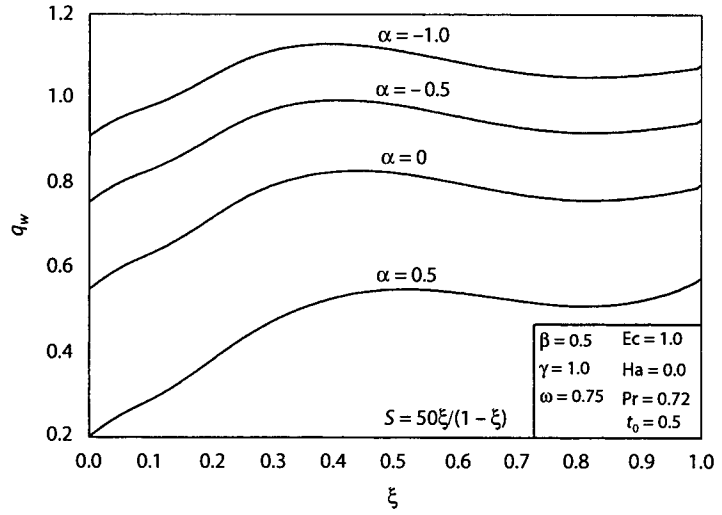

Fig. 18. Effects of α on wall heat transfer.

Conclusion

Continuum equations governing steady, laminar, hydromagnetic, compressible, boundary-layer flow and heat transfer of a two-phase paniculate suspension past a non-isothermal semi-infinite flat plate are developed. A boundary-layer order of magnitude analysis revealed that the particle-phase density in the boundary layer is uniform. This fact allowed a great simplification of the problem and was in marked contrast with previously published work on the incompressible and compressible versions of the problem.

The resulting boundary-layer equations which allow for particle-phase viscous stresses, fluid-phase heat generation or absorption, and the magnetic body force were solved numerically using a standard implicit finite difference method. The inclusion of the particle-phase stresses required the imposition of a wall boundary condition on the tangential velocity for the particle phase. While the exact form of such boundary conditions is unknown at present, a boundary condition similar to that usually employed in rarefied gas dynamics with the wall slip coefficient being a function of the tangential distance of the plate was utilized. The numerical results revealed that the presence of a moving transverse magnetic field normal to the flow direction resulted in decreasing the displacement thicknesses of both phases and increasing their skin-friction coefficients and the wall heat transfer coefficient. In addition, it was found that the particulate wall slip coefficient had significant effects on results especially those associated with the particle phase. Furthermore, it was predicted that heat generation reduced the wall heat transfer while heat absorption augmented it and that the wall heat transfer is more responsive to heat generation than to heat absorption.

REFERENCES

Blottner, F. G., 1970, Finite-Difference Methods of Solution of the Boundary-Layer Equations, *AIAA Journal*, **8**, pp. 193–205.

Chamkha, A. J., 1996a, Compressible Dusty-Gas Boundary-Layer Flow Over a Flat Surface, *ASME Journal of Fluids Engineering*, **118**, pp. 179–185.

Chamkha, A. J., 1996b, Compressible Two-Phase Boundary-Layer Flow with Finite Particulate Volume Fraction, *International Journal of Engineering Science*, **34**, pp. 1409–1422.

Chamkha, A. J. and Peddieson, J., 1994, Boundary-Layer Theory of a Paniculate Suspension with Finite Volume Fraction, *ASME Journal of Fluids Engineering*, **116**, pp. 147–153.

Chamkha, A. J. and Peddieson, J., 1989, Boundary-Layer Flow of a Particle-Fluid Suspension Past a Flat Plate, *Developments in Mechanics*, **15**, pp. 315–316.

Chamkha, A. J. and Peddieson, J., 1990, *Boundary-Layer Theory for a Particulate Suspension with a Finite Volume Fraction*, Engineering Science Preprint Number 27.90005, 8 pages.

Chamkha, A. J. and Peddieson, J., 1992, Singular Behavior in Boundary-Layer Flow of a Dusty Gas, *AIAA Journal*, **30**, pp. 2966–2968.

Datta, N. and Mishra, S. K., 1982, Boundary Layer Flow if a Dusty Fluid Over a Semi-Infinite Flat Plate, *Acta Mechanica*, **42**, pp. 71–83.

Gadiraju, M., Peddieson, J., and Munukuttia, S., 1992, Exact Solutions for Two-Phase Vertical Pipe Flow, *Mechanics Research Communications*, **19**, pp. 7–13.

Gidaspow, D., 1986, Hydrodynamics of Fluidization and Heat Transfer: Super Computer Modeling, *Applied Mechanics Reviews*, **39**, pp. 1–23.

Marble, F. E., 1970, Dynamics of Dusty Gases, *Annual Review of Fluid Mechanics*, **2**, pp. 297–446.

Osiptsov, A. N., 1980, Structure of the Laminar Boundary Layer of a Disperse Medium on a Flat Plate, *Fluid Dynamics*, **15**, pp. 512–517.

Patankar, S. V., 1980, *Numerical Heat Transfer and Fluid Flow*, McGraw-Hill, New York.

Prabha, S. and Jain, A. C., 1980, On the Use of Compatibility Conditions in the Solution of Gas Particulate Boundary Layer Equations, *Applied Scientific Research*, **36**, pp. 81–91.

Singleton, R. E., 1965, The Compressible Gas-Solid Particle Flow Over a Semi-Infinite Flat Plate, *ZAMP*, **16**, pp. 421–449.

Soo, S. L., 1968, Non-Equilibrium Fluid Dynamics-Laminar Flow Over a Flat Plate, *ZAMP*, **19**, pp. 545–563.

Soo, S. L., *Paniculate and Continuum: Multiphase Fluid Dynamics*, Hemisphere Publishing Corporation, New York, 1989.

Wang, B. Y. and Glass, I. I., 1988, Compressible Laminar Boundary-Layer Flows of a Dusty Gas Over a Semi-Infinite Flat Plate, *Journal of Fluid Mechanics*, **186**, pp. 223–241.

□◆◆◆□